Ultrasensitive quantification of Extracellular Vesicle Cargo, Size and Morphology using SMLM

SUMMARY

Investigating Extracellular Vesicle (EV) cargo improves our understanding of intercellular communication and the roles of EVs in homeostatic or physiopathological processes. Single molecule localization microscopy (SMLM) enables researchers to gain valuable insights into EV mechanisms, function, their molecular cargo and associated biomarkers.

The Application Kit: EV Profiler 2™ together with the Nanoimager enables:

- Profiling of EV populations down to the single-EV level
- Quantification of EVs and their biomarkers, with 20 nm resolution
- EV sizing and morphological identification using a generic Pan-EV stain
- Detection of cargo molecules contained within EVs using permeabilization

INTRODUCTION

EVs are lipid bilayer-enclosed particles from 30 to 1000 nm in diameter released by all cell types, critical for tissue homeostasis, and cell-to-cell communication during development and health changes. EVs are also unique carriers of disease state markers such as RNA, DNA, cytosolic or membrane-bound proteins, and other signaling factors[1]. Their cargo-loading capabilities have attracted interest in EVs as vehicles for drug-based cell targeting, vaccine delivery, and biomarker research in cancer and viral infections, among others[1-4]. In-depth study of EV cargo molecules can reveal important information on donor cell type, EV biogenesis, and donor cell metabolic and disease state[5]. Current methods, including western blots, dot blots, and flow cytometry, often rely on bulk measurements averaging large EV populations. Even within a single purification from a single source, EV samples are highly heterogeneous, which can lead to misrepresentation of EV subpopulations and cargo distribution when using bulk analysis methods.

Super-resolution microscopy provides ten times better resolution compared to traditional microscopy, allowing imaging of single EVs and their biomarkers with 20 nm precision. Single-molecule localization microscopy (SMLM), an umbrella term for a variety of techniques that enable super-resolution imaging of EVs, allows researchers to gain insight into EV size and shape, while simultaneously detecting internal cargo or surface biomarkers. In turn, it allows for a greater understanding of how cargo sorting may impact size, and provides insights into EV biogenesis pathways. Here, we used ALG-2 interacting protein X (ALIX), a well-characterized cargo protein contained in many EVs types and implicated in tetraspanin recruitment[6], to illustrate how to SMLM to probe for cargo molecules of interest, understand the impact of permeabilization on EV integrity, and the relationship between cargo-loading and EV size.

CHALLENGES

Detection of EV cargo can be challenging, particularly when combined with super-resolution imaging, where the cargo signal needs to be precisely localized. The small size of EVs also poses a challenge for cargo detection on a single-EV basis. Many traditional detergents create large pores relative to the size of the EV, which can result in degradation of smaller EVs with a limited membrane amount. This event known as "over-permeabilization" can lead to inaccurate internal cargo quantification and excessive background in SMLM caused by membrane fragments scattered across the surface.

To ensure accurate detection, morphology assessment and sizing of EVs, it is important to use a generic membrane stain that binds all EVs. Many commonly used membrane markers, such as wheat germ agglutinin (WGA) or concanavalin A (ConA), are lectins that bind to glycans, which make membrane visualization dependent on glycosylation. Here, we used the EV Profiler 2 kit Pan-EV stain, which offers membrane visualization independently of protein expression or membrane glycosylation (Figure 1).

Importantly, validation of a cargo marker requires a variety of control experiments to ensure high sensitivity detection of low-abundance molecules, EV integrity after permeabilization, accurate EV sizing, and quantification of particles positive for the marker without bias. These controls support the reliability and reproducibility of SMLM EV data and may include some or all of the following: a non-permeabilization control, lyzed EVs, an isotype control or detection of antigen not found in EVs, and cell staining.

Learn more details about these at https://insights.oni.bio/blog.

METHODS

PANC1 cells were cultured in phenol red-free DMEM supplemented with 10% EV-depleted FBS and 1% penicillin/streptomycin. Conditioned medium was collected after 48 hours, spun to remove cellular debris, and concentrated to 400 µL using Vivaspin™ 20 100 kDa concentrators at 1000 x g in 10-minute intervals.

Concentrated medium was loaded into IZON qEVoriginal Gen 2 70 nm column equilibrated with ONI's Wash Buffer. SEC collection was performed manually, using gravity flow. 3 mL of void volume was discarded, then 500 µL of fractions 7-10 were collected off the qEVoriginal column. Fraction 7 was used for subsequent preparation using ONI's EV Profiler 2 kit. EVs were captured using PS Capture and labeled using the Pan-EV + Tetraspanin Trio + custom marker detection modality. ALIX was detected using a recombinant rabbit monoclonal antibody from EV Profiler 2. Staining Solution from ONI's dSTORM Training Kit was used as the rabbit anti-Nup98 control, and a rabbit isotype control was purchased. All cargo antibodies were directly conjugated to AlexaFluor™ 647.

Imaging was performed on a Nanoimager Mark II S microscope using NimOS software. Analysis was performed using ONI's CODI software with preset "Pan-EV + custom marker" analysis settings. The DBSCAN algorithm was used to cluster localization data, using localizations from the Pan-EV and Tetraspanin Trio stains. Data were plotted using Graphpad Prism 10.2.2.

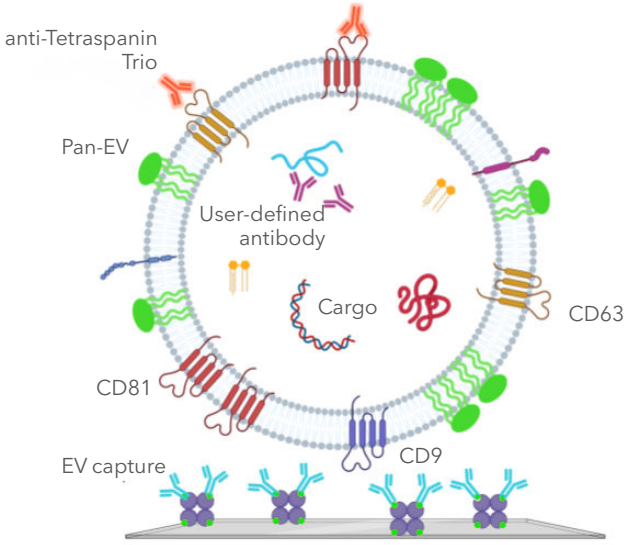

Figure 1 | Schematic representation of the EVs captured and stained using the ONI's EV Profiler 2 kit.

RESULTS

PANC1 EVs were captured on the EV Profiler 2 assay chip using Phosphatidylserine (PS) Capture. Six chips were used, with six lanes being stained for Nup98, six lanes being stained with an Isotype Control, and 12 lanes stained for ALIX. All lanes were also stained with ONI's Pan-EV stain and Tetraspanin Trio for accurate vesicle sizing and identification, in alignment with the MISEV guidelines[7]. Four fields of view (FOVs) were imaged per lane. Data was analyzed using the EV Profiler 2 kit presets available in ONI's CODI.

A significant increase in visibly ALIX-positive EVs was observed in permeabilized samples compared to little visible signal without permeabilization, as expected (Figure 2A). Quantification revealed the clusters positive for the AlexaFluor™ 647 marker of interest (Nup98, Isotype Control, or ALIX, respectively), whereby the detected levels of Nup98 and Isotype Control were very similar to those of ALIX detected without permeabilization. This suggested that 1-2% of detection is false-positive noise of the assay. A statistically significant increase in the percentage of ALIX-positive clusters occurred after sample permeabilization (Figure 2B), albeit heterogeneity was observed between FOVs. The mean level of ALIX positivity in non-permeabilized samples was 1.5% compared to 8.2% when permeabilized. Small increases in positivity also occurred after permeabilization for Nup98 (1.4% vs 2.2%) and the Isotype Control (1.4% vs 2.4%), although these were not statistically significant.

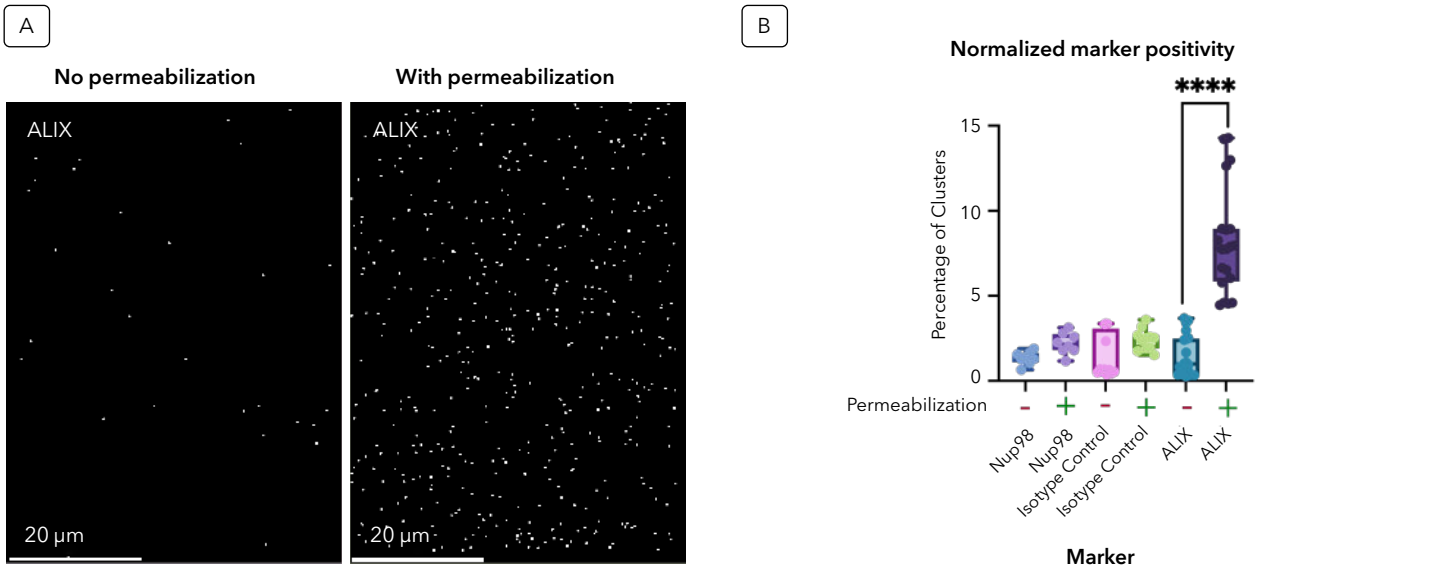

Figure 2 | Significant increase in ALIX signal after permeabilization. A) Representative images of a whole FOV, with only the ALIX signal shown. Left image is a non-permeabilized sample; the right image is a permeabilized sample. B) Percentage of clusters positive for the marker labeled with AlexaFluor™ 647. Each FOV was normalized to total clusters in the FOV; each point represents an FOV. **** = p<0.000001, unpaired t-test.

ONI's EV Profiler 2 kit relies on a membrane stain to size EVs accurately, and permeabilization causes physical changes in the membrane. Thus, it is crucial to check whether permeabilization is altering the diameters of the EVs detected in each sample. Here, no apparent visual difference was observed in the Pan-EV stain between permeabilized and non-permeabilized samples (Figure 3A and 3B). Accordingly, the data showed no significant difference in the diameters detected across EVs regardless of marker stained and permeabilization status (Figure 3C). This indicates that EVs were intact after permeabilization. Within the permeabilized sample stained for ALIX, the diameter of ALIX-positive (ALIX+) and ALIX-negative (ALIX-) EV populations was plotted. In this case, the data showed a significant difference between the diameters of EVs positive for ALIX, with EVs being slightly larger than in the ALIX-negative population (249 ± 151 nm vs 191 ± 132 nm). These data can be represented as a relatively frequency histogram (Figure 3D), emphasizing that the entire ALIX+ EV population tends to be slightly larger than the ALIX- one, with considerable overlap between the two populations. This may indicate that ALIX is preferentially packaged into larger EVs, or that the presence of ALIX results in larger EVs.

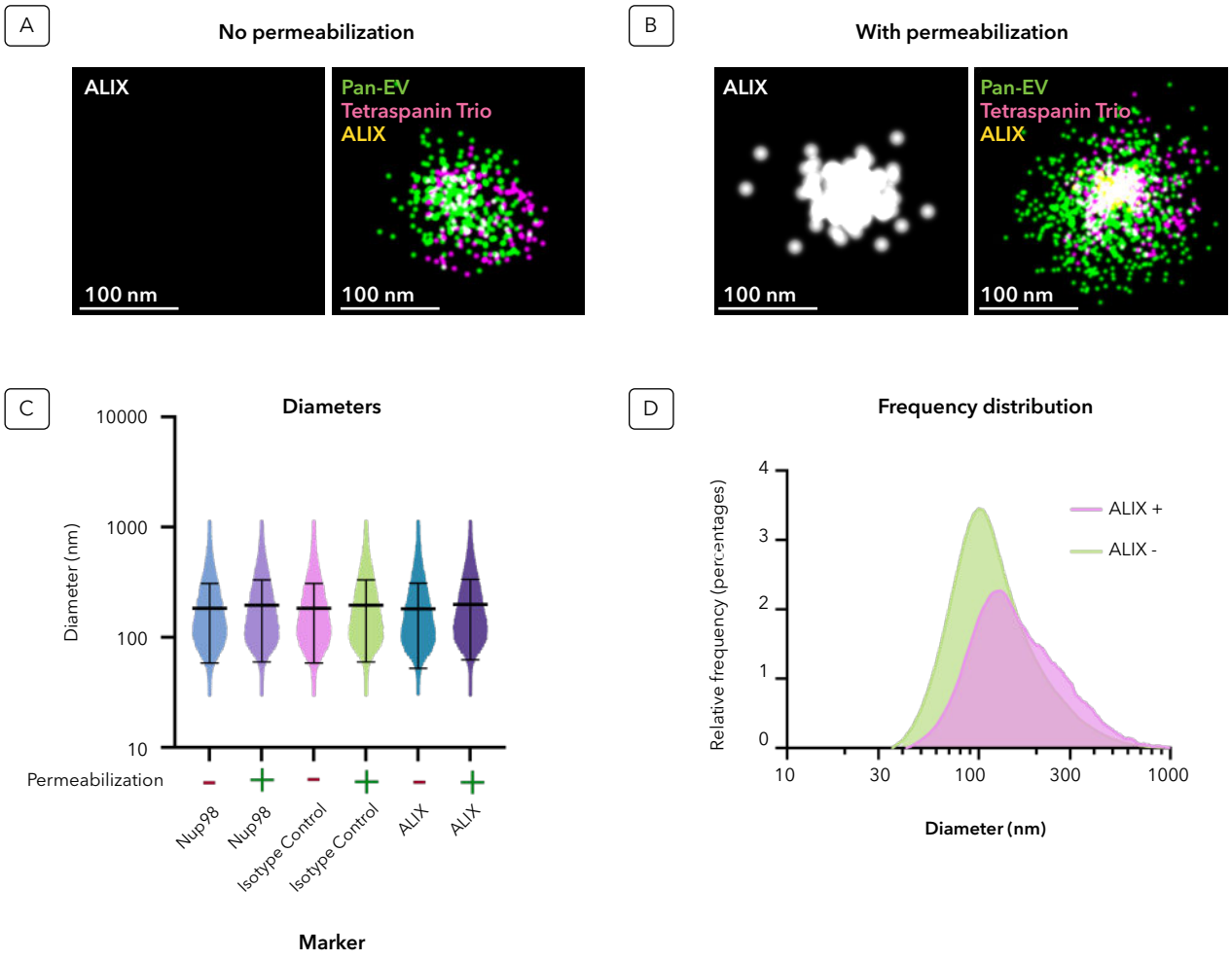

Figure 3 | Permeabilization does not significantly change EV diameter, ALIX+ EVs are larger. A and B) Representative images of single EVs that were non-permeabilized (A) or permeabilized (B) and stained for ALIX. C) EV diameters detected using ONI's Pan-EV stain, the mean with SD was plotted on a logarithmic scale to display the range of EV sizes. D) Histogram of the relative frequency of the diameter of ALIX positive (ALIX+) and ALIX negative (ALIX-) EVs within permeabilized samples. A bin size of 5 nm was used for the histogram, and the resultant histogram was smoothed using second-order smoothing of 9 neighbors. The X-axis is shown on a log10 scale, the Y-axis shows the relative frequency of each bin as a percentage.

When performing SMLM using ONI's EV Profiler 2 kit and the Nanoimager, users can extract the number of biomarker localizations present in a single EV. While this cannot be exactly correlated to protein expression, the number of localizations generally correlates with protein content on an order of magnitude scale. Thus, we can investigate if EV size impacts the amount of ALIX present in an EV and if there is a correlation between the two parameters. Interestingly, the data suggested a characteristic size at which an EV will contain the most localizations of ALIX (Figure 4). EVs with the most ALIX were typically smaller than 500 nm but larger than 150 nm. This did not align with the median diameter, which is approximately 140 nm (right Y-axis, Figure 4). This may indicate that the presence of more ALIX results in larger EVs.

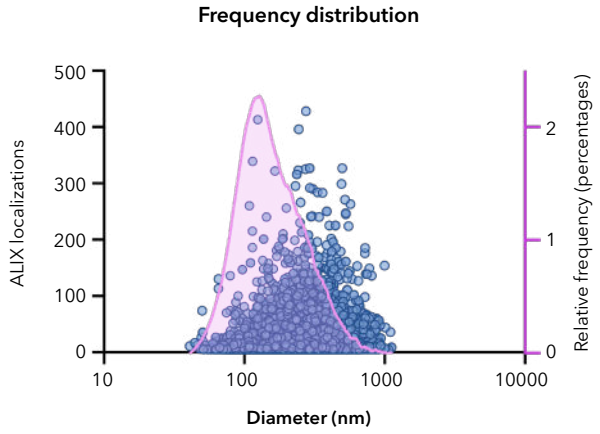

Figure 4 | ALIX+ EVs have a characteristic size. ALIX localizations (left Y-axis) vs. diameter, overlaid with relative frequency (right Y-axis, from figure 4D). A bin size of 5 nm was used for the histogram, and the resultant histogram was smoothed using second-order smoothing of 9 neighbors. The X-axis is shown on a log10 scale, the right Y-axis shows the relative frequency of each bin as a percentage.

CONCLUSIONS

Detection and quantification of EVs at the population and single-EV level can be challenging due to their small size, heterogeneous sample nature, and low-level of certain biomarkers such as cargo molecules contained within EVs. The EV Profiler 2 kit together with the Nanoimager and CODI software offers researchers an end-to-end solution to assess EV morphology and integrity, determine EV size, and detect and quantify low-abundance EV cargo and surface molecules.

The data shown here revealed a significant increase in ALIX signal after permeabilization and how ALIX+ EVs have a characteristic size, which may indicate a relationship between ALIX and EV size. Together with use of appropriate controls, users can ensure SMLM experiment reproducibility and reliability, and gather critical data on their EV cargo molecules of interest using custom antibodies.

REFERENCES

1. Dixson AC, Dawson TR, Di Vizio D. et al. Context-specific regulation of extracellular vesicle biogenesis and cargo selection. Nat Rev Mol Cell Biol 24, 454–476 (2023). https://doi.org/10.1038/41580-023-00576-0

2. Kim J, Lee SK, Jeong SY. et al. Cargo proteins in extracellular vesicles: potential for novel therapeutics in non-alcoholic steatohepatitis. J Nanobiotechnol 19, 372 (2021). https://doi.org/10.1186/s12951-021-01120-y

3. Katsuda T, Kosaka N, Ochiya T, The roles of extracellular vesicles in cancer biology: Toward the development of novel cancer biomarkers. Proteomics 14, 412-425 (2014). https://doi.org/10.1002/pmic.201300389

4. Hurwitz SN, Rider MA, Bundy JL. et al. Proteomic profiling of NCI-60 extracellular vesicles uncovers common protein cargo and cancer type-specific biomarkers. Oncotarget. 7(52):86999-87015 (2016). https://doi.org/10.18632/oncotarget.13569

5. Yates AG, Pink RC, Erdbrügger U. et al. In sickness and in health: The functional role of extracellular vesicles in physiology and pathology in vivo: Part I: Health and Normal Physiology: Part I: Health and Normal Physiology. J Extracell Vesicles. 11(1):e12151 (2022). https://doi.org/10.1002/jev2.12151

6. Larios J, Mercier V, Roux A. et al. ALIX- and ESCRT-III–dependent sorting of tetraspanins to exosomes. J Cell Biol. 219 (3) (2020). https://doi.org/10.1083/jcb.201904113

7. Welsh JA, Goberdhan DCI, O'Driscoll L., et al. Minimal information for studies of extracellular vesicles (MISEV2023): From basic to advanced approaches. J Extracell Vesicles. 13(2):e12404 (2024). https://doi.org/10.1002/jev2.12404.